Development of an Instrumented Channel for Multiphase Flow in Unsaturated Soils

R.P. Sousa, I.B. Oliveira, S.L. Machado, E.A. Sales

Abstract. This paper presents the development of an instrumented channel for two-dimensional multiphase flow of automotive fuels in unsaturated soils. Flow experiments were performed using water or diesel in an eolian sand at residual water saturation, a particular case of multiphase flow. Aspects such as the visual monitoring of the infiltration experiments and the great reproducibility of the developed experimental protocol can be cited as highlights of this research. The two sets of tensiometers, hydrophilic and hydrophobic, used during the diesel experiment, responded differently. While the hydrophobic tensiometer, filled with diesel, measured the full range of diesel suctions, the hydrophilic tensiometers, filled with water, responded less effectively to the passage of the diesel wetting front. Flow experiments were modeled using Philip's equation, considering the flow in unsaturated conditions above the wetting front. The time required for the diesel wetting front to reach the tensiometers was about 8.8 times higher than for water, considering the tensiometer readings, and, about 6.1 times higher than for water considering the visual observations. These values are comparable to the ratio of fluid mobilities $[(\rho_w/\rho_w)/(\rho_{diesel}/\rho_{diesel}) = 5.5]$ of water and diesel.
Keywords: physical modeling, unsaturated soils, multiphase flow.

1. Introduction

Since the seventies, many theoretical and experimental studies have been performed to describe the flow and solute transport of non-aqueous phase liquids (NAPL) through unsaturated soil, the capillary fringe and within the aquifer, as reviewed by Abriola (1989). Abriola & Pinder (1985) elaborated the first mathematical and computational code to model the flow of NAPL in the subsurface, a very complete multiphase and multi-component 3D model, considering mass transfer between phases. Kaluarachchi & Parker (1989) developed a multiphase 3D model for the flow through both saturated and unsaturated zones. Concerned about the predictive ability of the numerical models, Kueper *et al.* (1989) highlighted the need for experimental studies in order to understand the multiphase flow under various hydrogeological conditions, as the predictions have to be compared with data obtained in the laboratory or in the field.

The literature reports the development of many experimental devices used to generate data to model multiphase flow. For example, Silliman *et al.* (2002) presented the development of two-dimensional experiments on solute transport in the capillary fringe of homogeneous and heterogeneous porous media. McDowell & Powers (2003) analyzed the distribution of gasoline with 10% alcohol by volume in a two-dimensional flow study conducted in the vadose zone and capillary fringe. The authors used imaging techniques, with emphasis on the partitioning of ethanol in the different soil phases. The experimental work of Kamon *et al.* (2004) characterized the flow of DNAPL in the saturated zone, both considering or not the groundwater flow. The works of Oostrom *et al.* (2007) and Kamaruddin *et al.* (2011) present a comprehensive review of many laboratory and numerical studies on the migration of hydrocarbons in the subsurface environment, with an emphasis on DNAPL and LNAPL infiltration and redistribution.

Other examples of laboratory experiments performed in flow channels made use of different techniques to measure the transport parameters (Schiegg, 1990; Host-Madsen & Jensen, 1992; Oliveira, 1995; Butts & Jensen, 1996; Schroth *et al.,* 1998; Kamon *et al.,* 2004; and Kechavarzi *et al.,* 2000, 2005, 2008). The techniques described in these works are invasive and non-invasive. The non-invasive techniques used for soil moisture content determination are: X-ray and gamma ray attenuation, visible light reflection and transmission through the soil, analysis of multispectral images, radar (GPR) and three-dimensional seismic methods. The invasive techniques used for suction measurements are: tensiometry and electrical conductivity. The various liquids used by the researchers were: water, ethylene glycol, 4-clorotoluene, n-hexanol, mineral oil, hydrofluoreter, BTEX, gasoline, Soltrol 220® and Jet Fuel, in different types of soils.

Riseuda Pereira de Sousa, PhD Student, Industrial Engineering Program, Universidade Federal da Bahia, Salvador, BA, Brazil. e-mail: riseuda.sousa@gmail.com.
Iara Brandão de Oliveira, PhD, Associate Professor III, Environmental Engineering Dept., Universidade Federal da Bahia, Salvador, BA, Brazil. e-mail: oliveira@ufba.br.
Sandro Lemos Machado, PhD, Associate Professor III, Materials Science and Technology Dept., Universidade Federal da Bahia, Salvador, BA, Brazil. e-mail: smachado@ufba.br.
Emerson Andrade Sales, PhD, Associate Professor II, Physicochemical Department, Universidade Federal da Bahia, Salvador, BA, Brazil. e-mail: eas@ufba.br.
Submitted on January 20, 2012; Final Acceptance on January 21, 2013; Discussion open until April 30, 2013.

In Brazil, many researchers (Corseuil & Marins, 1997; Kaipper, 2003; Silveira, 2004; Schneider, 2005; Amorim Jr, 2007) have been developing experimental studies on soil and aquifer contamination by Brazilian automotive fuels. However, most of these studies are developed in the field in the southeast region of Brazil and they focus on NAPL transport after reaching the water table.

To generate specific data for multiphase flow of Brazilian automotive fuels in a variety of unsaturated soils, the present research developed a two-dimensional instrumented channel to carry out laboratory studies of NAPL transport in unsaturated soils. It is planned to test soils collected in the Metropolitan area of Salvador: sand dune (non reactive soil); regolith (sandy silty clay soil); tertiary sediments (clayey sand soil); and an expansive clay soil. This paper describes the development and testing of the experimental apparatus, using water and diesel as the permeating fluids, at residual water saturation, and sand dune as the porous medium. Future studies will address diesel permeation through the other three soil types, useful information for describing the Brazilian automotive fuel contamination in the studied tropical region, information not available in the literature.

2. Materials and Methods

2.1. Soil and liquid characteristics

The soil used in the experiments is a Quaternary sand dune from the Metropolitan Region of Salvador, state of Bahia, Brazil, with 100% of sand content, classification NBR 6502 - medium to fine sand and classification SUCS - SP poorly graded sand. The sand has a grain density of $\rho_s = 2.68$ g/cm^3 and an organic content given in total volatile solids of TVS = 0.091%. Grain size distribution and soil liquid retention curves are presented in Figs. 1 and 2, respectively.

For the soil water retention curves and the infiltration experiments in the flow channel, drinking water distributed by the state company EMBASA was used, at equilibrium with the laboratory temperature and atmospheric pressure, after losing its residual chlorine. The recommendation for using tap water in the infiltration experiments, instead of demineralized water, was given by Philip (1969), Bond & Collins-George (1981) and Klute (1986) to avoid chemical aggressiveness. For the soil diesel retention curves and the infiltration experiments in the flow channel, commercial Brazilian diesel was used. From the literature, the properties of water and diesel at 29 °C, are given in Table 1.

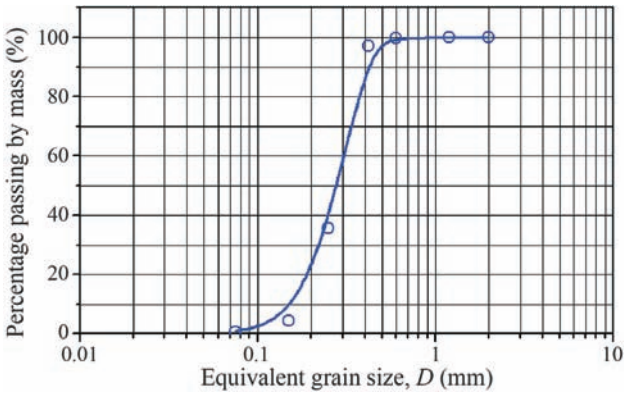

Figure 1 - Sand grain size distribution curve.

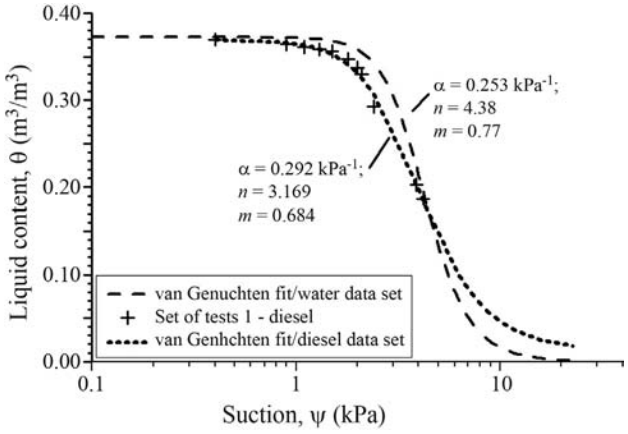

Figure 2 - Soil liquid retention curves (SLRC), drainage branch, using a vaporization chamber.

The soil liquid retention curves (SLRC) shown in Fig. 2 were obtained with a vaporization camera described in Sousa *et al.* (2011), a procedure applied by many authors (Plagge *et al.*, 1990; Wendroth *et al.*, 1993; Tamari *et al.*, 1993; and Oliveira, 1995). To apply this method, the saturated soil with the liquid of interest is open to the atmosphere and subject to a gradual loss of liquid content. The suction measurements are made sequentially, using tensiometers, at the different stages of the drying process. Further information about this procedure can be obtained in

Table 1 - Liquid properties at 29 °C from Oliveira (2001).

Liquids	Density ρ (g cm^{-3})	Viscosity μ (cP)	Mobility ρ/μ (g cm^{-3}/cP)	Dielectric constant ε	Vapor pressure PV (mmHg)	Surface tension σ (dina cm^{-1})
Water	0.9954	0.810	1.229	80.08	32.238	71.38
Diesel	0.8323	3.75	0.222	2.13	2.46 E-4*	26.78*

*Reference: Environmental Canada, ESTC (1997).

Sousa *et al.* (2011). The Van Genuchten (1980) model was used to fit the soil liquid retention curves as follows:

$$\Theta = \frac{1}{\left[1+(\alpha\psi)^{n}\right]^{m}}, \quad (1)$$

with $\Theta = \frac{\theta - \theta_r}{\theta_s - \theta_r}$.

where θ, θ_s and θ_r [-] are the soil volumetric liquid content at a given suction ψ [kPa], at saturation and at residual state, respectively. α [kPa^{-1}], *m* [-] and *n* [-] are fitting parameters. $m = 1 - 1/n$ was adopted. The fitting curve for the soil water retention curve (SWRC) was obtained combining three different sets of suction and water content data.

Table 2 presents some physical parameters for the sand dune used in the experiments and the fitting parameters for each individual SLRC.

2.2. Soil compaction protocol

To assure the homogeneity of the sand within the flow channel, a compaction protocol was developed. For this, a small chamber was built with dimensions and materials similar to those used for the flow channel. The chamber was made of 8 mm thick glass, with dimensions of 40 x 40 x 13.5 cm. The procedure from Oliveira *et al.* (1996) was used to compact the soil inside the chamber and the flow channel. For this, thin layers of air dried sand were spread inside the chamber, followed by pressuring each layer with a 4 kg metal compactor until it reached a thickness of about 4 mm and the desired bulk density: $\rho = 1.72$ g/cm^3. In the case of the channel, each sand layer was uniformly distributed in the cross section and homogeneously pressured by a 7 kg metal compactor 270 times to achieve the same layer thickness and bulk density.

To verify the efficiency and reproducibility of the compaction protocol and to determine the soil capillary rise curve prior to the channel tests, capillary rise experiments were performed. In the compaction chamber, the water level was kept constant using two Mariotte tubes at each side. A layer of Geodrain (MacDrain 2L, Maccaferri of Brazil LTDA, Sao Paulo, SP) was used to uniformly distribute the water at the bottom. At the end of the experiment, soil samples were collected along the vertical profile to determine the soil bulk density and the moisture content. This procedure enabled the determination of the wetting branch of the soil water retention curve.

2.3. Flow channel

The channel is made of stainless steel and glass, with nominal dimensions of 200 x 120 x 15 cm (Fig. 3).

A channel thickness of 15 cm was chosen to follow the recommendation of Schiegg (1990) to avoid the wall effect, using a maximum value for sand diameter of 2 mm. The channel sides and front walls are made of a 12 mm thick tempered glass to enable visual observation of the experiments. The channel extensions located on each side wall were built to hold two Mariotte tubes for water application at the channel bottom. To prevent plastic deformation of the channel front side, two steel bar lattices were used (Fig. 3). To avoid undesirable physico-chemical interactions between the organic liquids and the stainless steel and the consequent wall effects, the inner surfaces of the channel, the bottom and back walls were coated with epoxy and covered with a thin layer of sand, ensuring mineralogical similarity with the porous medium.

A total of 30 holes, with couplings made of aluminum, were made in the back wall of the channel to insert tensiometers for suction readings: 15 for water (A) and 15 for NAPL (G). During the soil compaction, the openings were kept closed with aluminum caps, and during the installation of the tensiometers the caps were carefully removed to avoid soil loss, mainly for sand dune, a cohesionless soil. The openings also allow soil sampling using small aluminum tubes with nominal sizes of 15 x 0.635 cm (internal diameter). The samples are used for liquid content measurement at the end of the experiment.

In order to allow water or NAPL infiltration at the soil surface, a stainless steel reservoir was built, with a porous bottom made of sintered bronze, nominal pore size of 5 μm (Free Filters Industry and Commerce, Sao Paulo, SP, Brazil). A pressure transducer was installed inside the reservoir, just above the porous bottom, to monitor the liquid level during the experiments (Fig. 4).

The reservoir has dimensions of 50 x 20 x 15 cm with a storage capacity of about 15 L. After preliminary tests of

Table 2 - Physical parameters of sand dune obtained with vaporization cell and mathematical modeling.

Experiment number	Permeability coefficient k (m s^{-1})	Bulk density (kg.m^{-3})	Soil liquid retention curve				
			θ_r (m^3.m^{-3})	θ_s (m^3.m^{-3})	Fitting parameters van Genuchten (1980)		
					m (-)	n (-)	α (kPa^{-1})
#01 (water)	2.60 x 10^{-4}	1720	0.012	0.373	0.822	5.59	0.278
#02 (water)	2.60 x 10^{-4}	1724	0.015	0.371	0.803	5.08	0.222
#03 (water)	2.60 x 10^{-4}	1721	0.004	0.372	0.806	5.15	0.258
# 04 (diesel)	5.40 x 10^{-5}	1720	0.012	0.369	0.684	3.169	0.292

Figure 3 - View of the flow channel with sand compaction in progress. Features: steel bar lattice to reinforce the channel structure; back wall coated with epoxy & sand; sidewall reservoir to hold the Mariotte tube.

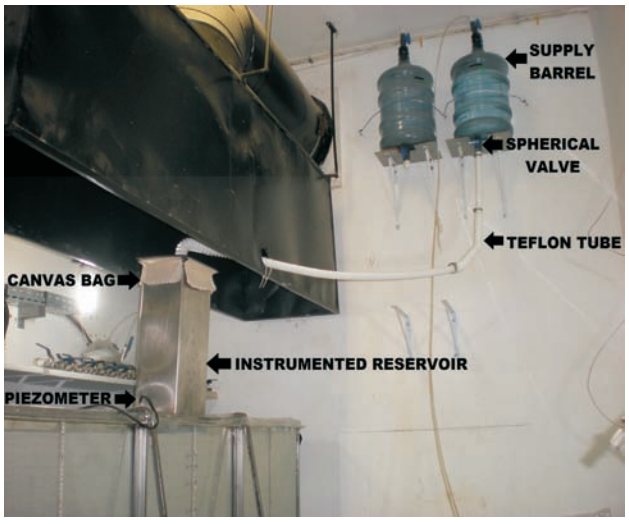

Figure 4 - Instrumented liquid reservoir on the soil surface connected to a fluid supply barrel.

the liquid reservoir performance with water, it was concluded that to maintain the water flow rate compatible with the sand infiltration rate it was necessary to use a canvas bag with column format inside the reservoir. For the diesel, a more viscous fluid, the canvas bag proved inadequate, and a plastic bag in column format was used. At the beginning of each infiltration experiment, a supply barrel, connected with the reservoir, dispenses the liquid through a Teflon tube with diameter of 29 mm (Fig. 4).

To measure interstitial pressures, hydrophilic and hydrophobic tensiometers were used. A detailed description of the tensiometer; the tensiometer calibration process; and the hydrophobic surface treatment for NAPL suction are presented in Sousa *et al.* (2011). For the infiltration experiments with water, hydrophilic tensiometers (filled with water) were used, whereas for diesel infiltration experiments both hydrophilic (filled with water) and hydrophobic tensiometers (filled with diesel) were used. The tensiometers consist of a pressure transducer with suction range from 0 to -100 kPa, connected to a stainless steel sleeve, with a porous tip made of alumina ceramic material (Model-0604D04 B01M1, Soilmoisture Equipment Corporation, USA). To saturate the tensiometers and its porous tips with the liquid of interest, a cylindrical vacuum chamber with nominal dimensions of 30 x 19.9 cm (internal diameter) was built in acrylic and aluminum. A high flow rate vacuum pump (Model D16A, Leybold Heraeus, 1 hp, Germany) extracts the air from the chamber. Figure 5 shows the 15 tensiometers inserted in the back wall of the channel to monitor the water infiltration test. To prevent the porous tips of the tensiometers from drying out, they must be inserted just before the test. A computer system (PLC Controller and Model-MCI02 QC, HI Technology Industry and Trade Ltda., Sao Paulo, SP, Brazil) for data acquisition and storage is connected to the tensiometers and the pressure transducer is located at the bottom of the liquid reservoir. Although not shown in this paper, the experimental apparatus has another set of tensiometers which are able to measure suction values of up to 1000 kPa (Epron EPX-NO1, Entran Sensors & Eletronics, Fairfield, NJ, USA), as described by Barreto *et al.* (2007). This set of tensiometers may be used in tests involving clayey soils.

2.4. Infiltration experiments and uni-dimensional modeling

Six infiltration experiments were performed, five with water and one with diesel. Table 3 shows the conditions observed for each of the six flow channel experiments. An average bulk density of $\rho = 1.714$ g/cm^3 was achieved for the six experiments, which is very close to the bulk density obtained in the compaction chamber ($\rho = 1.72$ g/cm^3), attesting the good reproducibility of the compaction protocol. At the beginning of each infiltration experiment, the supply barrel dispensed the liquid within the reservoir in about 25 s. Water/diesel interstitial pressures and the liquid level inside the reservoir were recorded every 2 s. The visual monitoring of the infiltration experiments was drawn by hand, tracing the successive wetting front positions on the channel front wall.

After finishing the experiments, soil samples were collected to determine the soil liquid contenth. The soil suc-

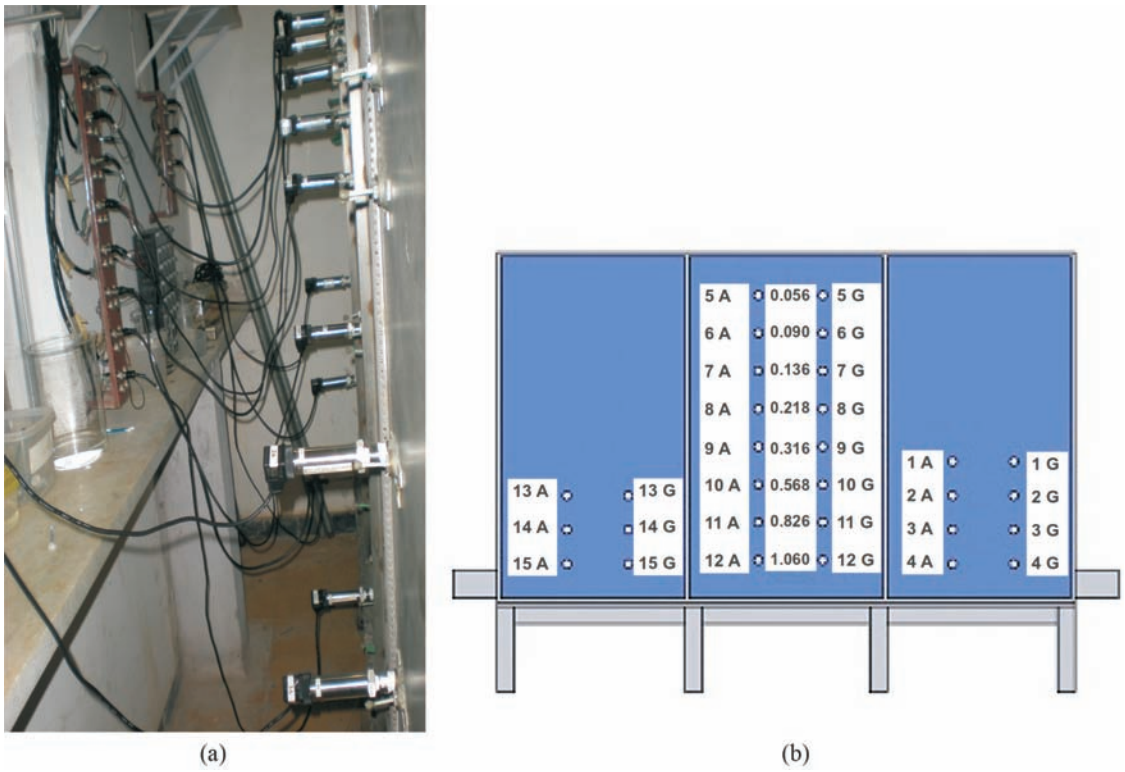

Figure 5 - (a) Channel back wall with attached tensiometers connected to the data acquisition system and (b) schematic view of the positions of the tensiometers. Numbers indicate the depth of the installed tensiometers (*m*).

tion values were recorded just before the removal of the tensiometers from the wall in order to determine a soil liquid retention curve (scanning curve). The water content was determined gravimetrically following the standard procedures. The diesel content was also determined gravimetrically, after keeping the samples in a muffle for 2 h at 600 °C (see Sousa *et al.*, 2011). The initial water and organic contents of the samples were discounted in order to compute the diesel content (the soil water content was assumed constant during the tests with diesel).

To simulate the advance of the wetting front for water and diesel, the infiltration model proposed by Philip (1969) was used, as follows:

$$I(t) = L(T)(\theta_s - \theta_i) = S\,t^{1/2} + \frac{2}{3}k\,t \qquad (2)$$

where $I(t)$ and $L(t)$ [L] are respectively the water infiltration and the wetting front position; k [LT^{-1}] is the coefficient of permeability; h_p and h_f [L] are the hydrostatic head at the soil surface and the suction head at the wetting front respectively; θ_i [-] is initial soil volumetric water content and S [$LT^{-1/2}$] is the soil sorptivity defined by Philip (1969) as follows:

$$S = \sqrt{2\,k(h_p - h_f)(\theta_s - \theta_i)} \qquad (3)$$

Table 3 - Some physical parameters related to the five flow channel experiments.

Experiment number	Soil height (cm)	Soil mass (kg)	Averaged bulk density (g cm^{-3})	Volume of liquid infiltrated (cm^{-3})	Elapsed time to reach capillary fringe (min)
#01- water	115	636.9	1.720	8813.0	25.3
#02- water	115	657.7	1.690	8205.2	30.6
#03- water	115	624.4	1.721	9420.8	31.1
#04- water	115	625.8	1.720	10940.2	31.1
#05- water	115	626.4	1.719	9420.8	29.4
#06- diesel	115	624.8	1.712	14524.5	214.0

The value of θ_s was assumed as the average soil porosity and θ_i was the average water content of the soil prior test beginning. Values of h_p were measured during the infiltration test by the pressure transducer installed at the bottom of the liquid reservoir. h_f was assumed as the average value of the initial tensiometer readings. The value of k was assumed as the average soil coefficient of permeability.

3. Results and Discussion

Figure 6 shows the wetting front advance for both water (experiment #05) and diesel (experiment #06). The lines were drawn on the front glass wall of the channel during the visual observation of the flow experiment. Isochrones approximately each 10 min are highlighted.

Considering the visual observations, the time for diesel wetting front to reach the capillary fringe was about 7.3 times longer than for water (214.0 min/29.43 min), a value slightly superior to the mobility ratio water/diesel $[(\rho_w/\rho_w)/(\rho_{diesel}/\rho_{diesel}) = 5.5]$.

Table 4 presents the time for the wetting front to reach the tensiometers from the tensiometer readings (TR) and from visual observation in the front face of the channel (VO).

It can be seen in Table 4 that for smaller depths, during the water infiltration experiments, the tensiometer detected the water front passage earlier than the visual observations, while the opposite occurred during the diesel experiment. This had been expected from the outset of the experiments. First, the water tensiometers responded quickly (1 to 3 s) to a change in the water pressure; and secondly, the water wetting front progresses so fast at the beginning of the infiltration that it was more difficult to draw the first two isochrones on the channel front wall. For the diesel, the wetting front progresses considerably slower than water, enabling better visual monitoring through the channel front wall, and the response time for the diesel tensiometers was about 35 s.

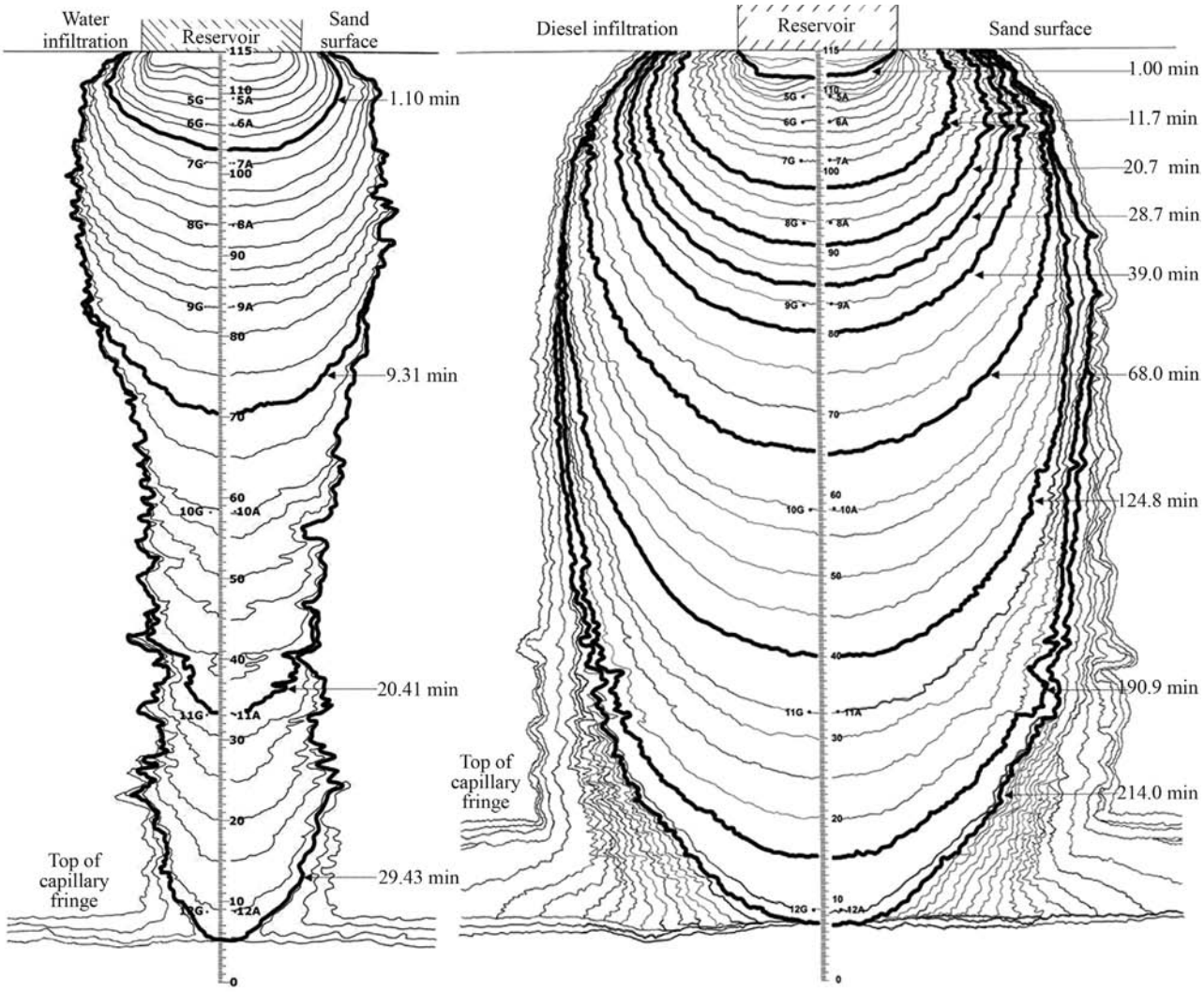

Figure 6 - Visual observation of the wetting front advance a) water experiment and b) diesel experiment.

Table 4 - Results for the time measurement from visual observations (VO) and that from tensiometer readings (TR).

Depth (m)	EXP#01 - Water			EXP#02 - Water			EXP#03 - Water			EXP#04 - Water			EXP#05 - Water			EXP - Diesel oil		
	Elapsed time			Elapsed time			Elapsed time			Elapsed time			Elapsed time			Elapsed time		
	V.O. (min.)	T.R. (min)	Diff. (%)	V.O. (min.)	T.R. (min)	Diff. (%)	V.O. (min.)	T.R. (min)	Diff. (%)	V.O. (min.)	T.R. (min)	Diff. (%)	V.O. (min.)	T.R. (min)	Diff. (%)	V.O. (min.)	T.R. (min)	Diff. (%)
0.056	0.28	0.23	15	0.60	0.57	6	0.29	0.18	38	0.24	0.27	-10	0.38	0.22	42	2.39	4.03	-69
0.090	0.61	0.42	32	1.00	0.68	32	0.62	0.25	60	0.65	0.43	34	0.71	0.38	46	3.96	5.67	-43
0.136	1.29	1.07	17	1.90	1.65	13	1.38	0.98	29	1.40	1.20	14	1.40	1.22	13	7.96	9.57	-20
0.218	2.74	2.68	2	3.82	3.40	11	2.93	2.42	18	2.69	2.87	-6	2.86	2.72	5	17.02	18.37	-8
0.316	4.88	6.45	-32	7.50	6.47	14	6.23	4.72	24	5.67	4.50	21	5.54	5.08	8	32.72	34.37	-5
0.568	11.44	17.58	-54	14.56	15.93	-9	16.13	12.85	20	14.55	12.90	11	13.35	11.88	11	83.77	86.97	-4
0.820	17.44	-	-	22.99	25.45	-11	24.14	21.05	13	22.71	20.60	9	20.91	19.58	6	142.9	-	-
1.062	24.08	-	-	30.37	28.45	6	0.00	29.18	-	30.02	28.87	4	28.45	27.15	5	209.14	232.07	-11

Notes: Elapsed time: time required for the wetting front to reach the tensiometer depth. Diff.: Difference between the visual observation and the tensiometer readings.

Figure 7 shows the progress of the wetting front position for the five water infiltration experiments. They are very close to each other (except test#01), attesting the reproducibility of the experiment. Figure 8 compares the results obtained for water and diesel, considering the wetting front from visual observations.

Figure 9 compares the readings of the tensiometers 5A, 7A and 8A for the five water infiltration experiments. Figure 9 shows that the tensiometers readings present good reproducibility. Although the initial suction measured by each tensiometer can be different, all tensiometers recorded the wetting front passage similarly. It also can be seen that 1 to 2.5 min after the passage of the wetting front, the suction increases gradually, indicating a drainage phenomenon. This is physically consistent with the fact that this is a variable head experiment and that infiltration velocities, lower than soil saturated permeability (see Fig. 12), will require some value of suction in the soil hydraulic function to equalize the infiltration rate.

Figure 10 shows the tensiometer readings (5G, 7G and 8G) for the diesel experiment. The arrows indicate the beginning of the drainage process. It can be seen that the tensiometer 8G did not become fully saturated, making it difficult to detect the soil drainage process. A comparison between Figs. 9 and 10 shows that for the diesel experiment the soil remained saturated for a longer period of time and the drainage process was much less pronounced.

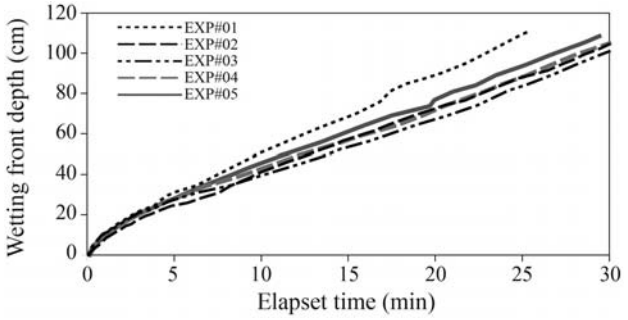

Figure 7 - Position of the water wetting fronts as a function of time.

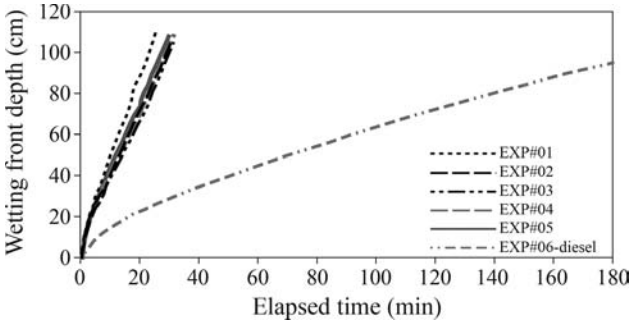

Figure 8 - Water and diesel wetting fronts position as a function of time (Visual observation).

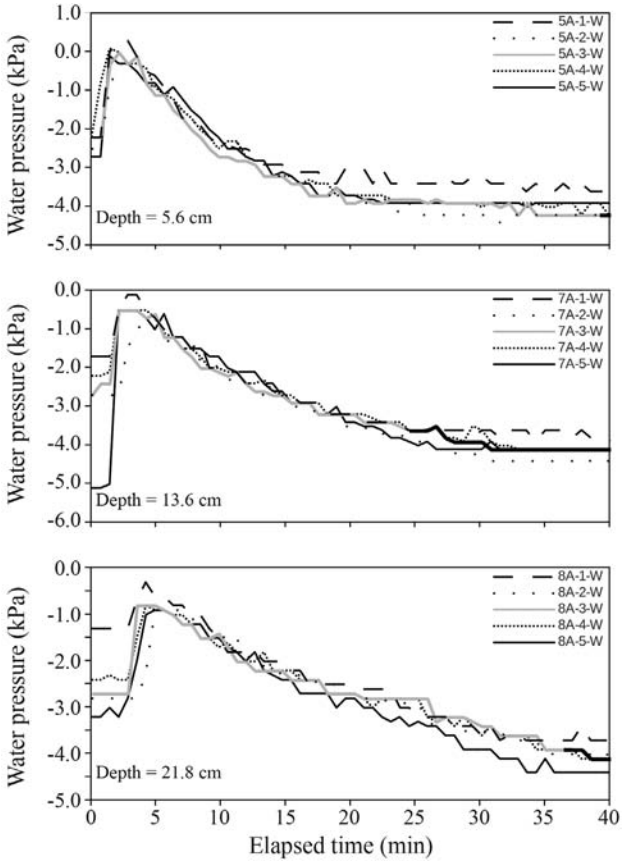

Figure 9 - Tensiometer readings in the performed water infiltration tests.

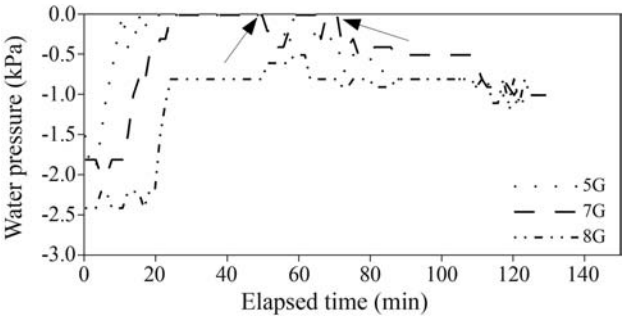

Figure 10 - Tensiometer readings in the diesel infiltration test.

Figure 11 compares the results of the average water interstitial pressure measurements in tensiometers 5, 7 and 8 (line A) to the obtained values in the diesel experiment (line G). The arrows in Fig. 11 indicate the passage of the wetting front detected by the diesel tensiometers. The ratios between the time required for the diesel wetting front to reach a tensiometer to that for water were 13.7 (tensiometer 5), 7.8 (tensiometer 7) and 6.5 (tensiometer 8) with an average value of 8.8. Greater ratios occurred for the shallower depths (also see Table 4, TR column). Considering the visual observations, an average value of 6.1 is obtained.

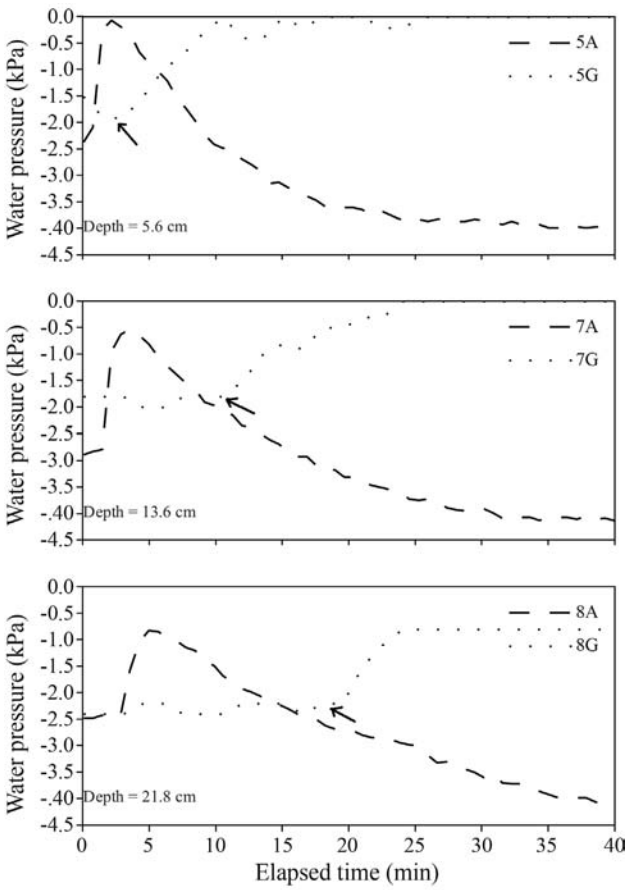

Figure 11 - Tensiometer readings in the water (average values) and diesel infiltration tests.

These results are comparable with the mobility ratio $[(\rho_w/\rho_w)/(\rho_{diesel}/\rho_{diesel}) = 5.5]$ of liquids, although they are slightly higher than that (see Table 1). The most probable explanation for this discrepancy is illustrated in Fig. 6. As can be observed, the spreading of the wetting front in the case of the diesel experiment is higher than that for water. This requires a higher infiltration volume on the soil surface to achieve the same depth below the surface, justifying why the time required for the diesel wetting front to reach the tensiometers was higher than expected.

Figure 12 shows the average infiltration rate and the average variation in the water head inside the reservoir as a function of time for the five water experiments. As can be observed, after 6.4 min the average infiltration rate goes below the soil saturated coefficient of permeability ($k_w = 2.60 \times 10^{-4}$ m/s). Figure 13 shows the same results as Fig. 12, now considering the diesel experiment. After only 75 min the infiltration rate goes below the soil saturated coefficient of permeability ($k_{diesel} = 5.40 \times 10^{-5}$ m/s).

The behavior observed in Fig. 12 for water is compatible with the drainage process illustrated in Fig. 9. The results presented in Fig. 13 indicate that the drainage process

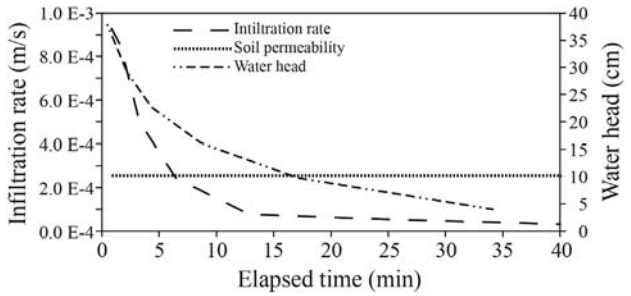

Figure 12 - Average values of infiltration rate and water head inside the reservoir for water infiltration tests.

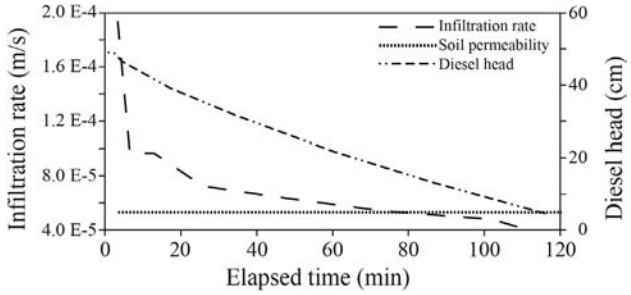

Figure 13 - Average values of infiltration rate and diesel head inside the reservoir for diesel infiltration tests.

in the diesel experiment is much less pronounced, which agrees with what is illustrated in Fig. 10.

The results presented in Figs. 7 and 8 were modeled with Philip's (1969) infiltration equation. In order to take into account the variations in the liquid head inside the reservoir (h_p) during the experiment, Eq. 2 was rewritten in an incremental way:

$$\Delta L = \frac{\dfrac{\partial L(t, h_p)}{\partial t}\Delta t + \dfrac{\partial L(t, h_p)}{\partial h_p}\Delta h_p}{\theta_s - \theta_i} \quad (4)$$

or

$$\Delta L = \frac{\left(0.5\, S\, t^{-\frac{1}{2}} + \frac{2}{3}k\right)\Delta t + \left(0.5\sqrt{2\,k(\theta_s - \theta_i)\,t}(h_p - h_f)^{-\frac{1}{2}}\right)\Delta h_p}{\theta_s - \theta_i} \quad (5)$$

Figure 14 presents the modeling results for the water infiltration tests (Exp#2, #3, #4 and #5). Average values of $\theta_s = 0.37$ and $\theta_i = 0.001$ were used for both liquids and the average value of h_f = -27 cm was adopted for water. The adopted values for h_p were those shown in Fig. 12. As can be observed, the use of the value of $k_w = 2.60 \times 10^{-4}$ m/s obtained in laboratory (Table 2) leads to an overestimation of the wetting front depth. This is probably due to the fact that in the case of the Philip' s equation a piston flow scenario is considered. In this scenario the infiltration rate is always higher than the saturated permeability of the soil and there is no drainage process, contrary to what was observed experimentally in this paper. In order to take into account the

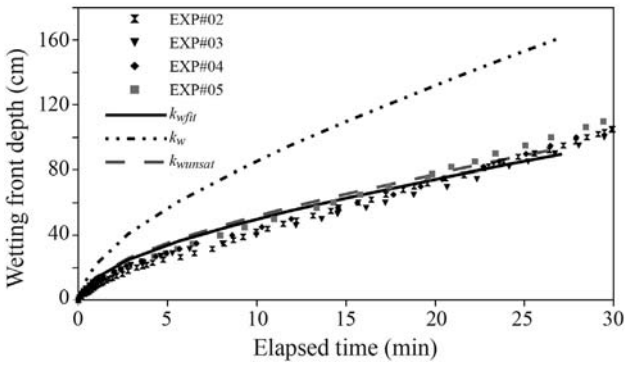

Figure 14 - Experimental results for water and curves modeled with Eq. 6.

occurrence of the drainage process in the performed tests a new value of k was adopted (k_{wunsat}) now considering the average value of soil suction during the drainage process. The Eqs 1 and 6 were used to compute a value of $k_{wunsat} = 1.21 \times 10^{-4}$ m/s, corresponding to a soil suction of 2.88 kPa.

$$k(\Theta) = k_{sat}\,\Theta^{\frac{1}{2}}\left[1 - \left(1 - \Theta^{\frac{1}{m}}\right)^{m}\right]^{2} \quad (6)$$

Figure 14 also presents the results of the model for the best fitting value of k ($k_{wfit} = 1.14 \times 10^{-4}$ m/s, $R^2 = 0.967$). This value is very close to the value of k_{wunsat}, which reflects the unsaturated conditions developed above the wetting front for all the water infiltration experiments.

Figure 15 presents the modeling results for the diesel infiltration test. An average value of h_f = -21.6 cm was adopted for diesel. The adopted values for h_p are shown in Fig. 13. As in the case of the water tests the value of $k_{diesel} = 5.40 \times 10^{-5}$ obtained in laboratory (Table 2) leads to an overestimation of the wetting front depth. A value of $k_{dunsat} = 4.27 \times 10^{-5}$ m/s was obtained considering an average value of suction of 1.16 kPa. In this case, the value of k_{dunsat} is closer to the value of k_{diesel} which is coherent with the fact that in the case of the diesel experiment the drainage process was much less evident. The wetting front advance is still overestimated in this

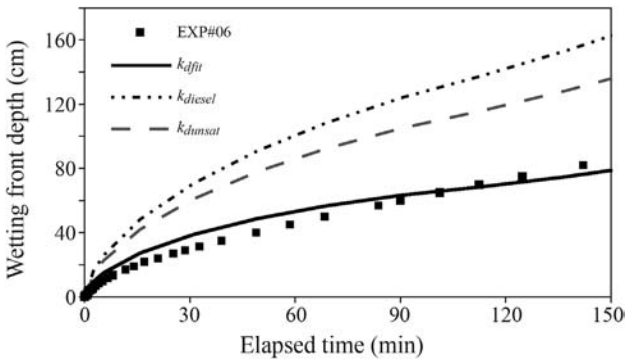

Figure 15 - Experimental and predicted results for diesel.

case even considering the value of k_{dunsat}. Again, the most probable explanation for this discrepancy is higher lateral spreading of the wetting front in the case of the diesel experiment. The best fitting of the experimental results yields a value of k_{dfit} = 2.03 x 10^{-5} m/s (R^2 = 0.956).

The values of the liquid content and suction measured at the end of the infiltration experiments were used to determine soil liquid retention curves for water and diesel. Table 5 summarizes the fitting parameters obtained. Figures 16 and 17 compare the soil liquid retention curves obtained at the end of the experiments with the main drainage retention curves presented in Fig. 2. As expected, the new curves are located to the left of the main drainage curve. However, the departure from the main drainage curve in Fig. 16 is much less remarkable than for the soil diesel retention curve (Fig. 17). This behavior agrees with the observations made above, based on Figs. 9 and 10, that in the water experiments the drainage process of the soil began earlier and was more evident than in diesel tests.

Figure 18 shows the results obtained when comparing the water and diesel tensiometer readings (7A and 7G) in the diesel experiment. As said above, the "A" tensiometers have a standard ceramic tip (hydrophilic) and are filled with water whereas the "G" tensiometers have a silanized ceramic tip (hydrophobic) and are filled with diesel. As can be observed, tensiometers "A" and "G" responded differently. While the hydrophobic tensiometer measured the full range of diesel suctions, the hydrophilic tensiometers responded less effectively to the diesel wetting front passage, showing the importance of using the hydrophobic tensiometer in the diesel experiments.

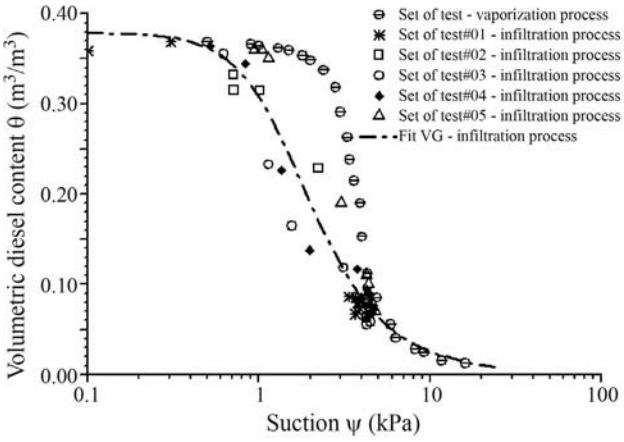

Figure 16 - Soil liquid retention curves for water.

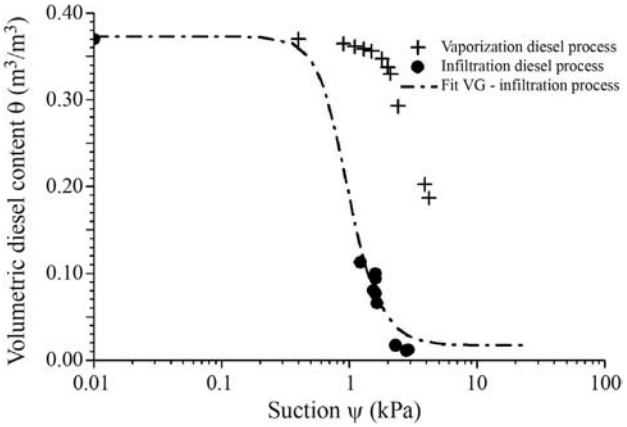

Figure 17 - Soil liquid retention curves for diesel.

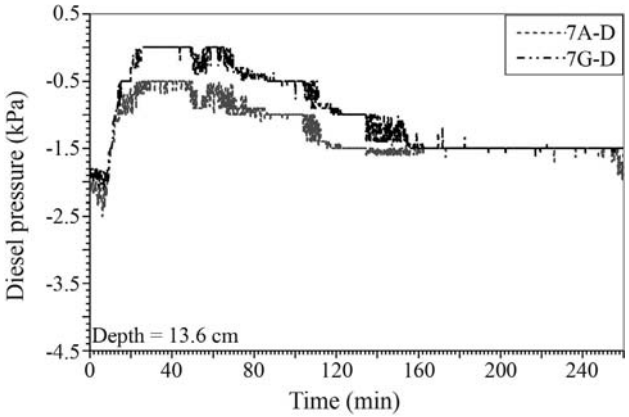

Figure 18 - Readings of the tensiometers 7A and 7G during diesel infiltration test.

Table 5 - Fitting parameters of the soil liquid retention curve using van Genuchten (1980) model.

Equipment	Experiment number	α (kPa^{-1})	m	n	θ_s (m^3.m^{-3})	θ_r (m^3.m^{-3})	R^2
Water experiments	#01	0.7984	0.5850	2.4120	0.3730	0.001	0.9870
	#02	0.6813	0.6180	2.3580	0.3840	0.001	0.9612
	#03	0.9782	0.5468	2.2067	0.3790	0.001	0.9677
	#04	0.7899	0.5588	2.2666	0.3711	0.001	0.9585
	#05	0.3931	0.7116	3.4675	0.3750	0.001	0.9930
	Fitting considering all data together	0.7047	0.5844	2.4064	0.3793	0.001	0.9377
Diesel experiment	#06	1.1497	0.7439	3.9052	0.3730	0.0171	0.9758

4. Conclusions

The infiltration experiments performed demonstrated the applicability of the instrumented channel to study multiphase flow in unsaturated soils. Aspects such as the use of tensiometers to measure the suction of water and diesel at the wetting front, the visual monitoring of the infiltration experiments and the great reproducibility of the developed experimental protocol are highlights of this research.

The experimental results for water and diesel were consistent with the theory of flow in non reactive granular soils. The liquid contribution for the flow is basically given by the fluid mobility as established by Nutting (1934). The average ratio between the time required for the diesel wetting front to reach a tensiometer, to that for water, was about 8.8. This result is slightly higher than the liquid mobility ratio [$(\rho_w/\rho_w)/(\rho_{diesel}/\rho_{diesel})$ = 5.5]. The most probable explanation for this discrepancy is the fact that the spreading of the wetting front in the case of the diesel experiment is higher than that of water, requiring a higher infiltration volume in the soil surface to achieve the same depth below the surface.

A good adherence was observed between the experimental and predicted results (R^2 = 0.967 for water and R^2 = 0.956 for diesel) when the infiltration process was modeled with the uni-dimensional infiltration equation proposed by Philip (1969). The use of the saturated value of permeability led to an overestimation of the wetting front depth both for water and diesel. This is probably due to the fact that in the case of the Philip' s equation a piston flow scenario is considered, which is contrary to what was observed experimentally in this paper. In order to take into account the occurrence of the drainage process in the performed tests a new value of k was adopted considering the average value of soil suction during the drainage process. In the case of the water experiments, the value of k_{wunsat} was able to reproduce the experimental data quite well. In the case of the diesel experiment, however, the value of k_{dunsat} still overestimated the experimental results. Again, the most probable explanation for this discrepancy is the higher lateral spreading of the wetting front in the case of the diesel experiment.

Notation

h_f = suction head at the wetting front, [L]
h_p = hydrostatic head at the soil surface, [L]
$I(t)$ = water infiltration, [L]
k = coefficient of permeability, [LT^{-1}]
k_w = water saturated coefficient of permeability, [LT^{-1}]
k_{wfit} = best fit for water coefficient of permeability, [LT^{-1}]
k_{wunsat} = unsaturated water coefficient of permeability, [LT^{-1}]
k_{diesel} = diesel coefficient of permeability, [LT^{-1}]
k_{dfit} = best fit for diesel coefficient of permeability, [LT^{-1}]
k_{dunsat} = unsaturated diesel coefficient of permeability, [LT^{-1}]
$L(t)$ = wetting front position, [L]
m = fitting parameter van Genuchten model (1980), [–]
n = fitting parameter van Genuchten model (1980), [–]
PV_{diesel} = diesel vapor pressure, [$M\,L^{-1}T^{-2}$]
PV_w = water vapor pressure, [$M\,L^{-1}T^{-2}$]
$S_{diesel/w}$ = diesel solubility in water
S = sorptivity, [$LT^{-1/2}$]
TVS = total volatile solids, [MM^{-1}]
α = fitting parameter van Genuchten model (1980); [LT^2M^{-1}]
ε_{diesel} = diesel dielectric constant [–]
ε_w = water dielectric constant [–]
μ_{diesel} = diesel liquid viscosity, [$M\,L^{-1}T^{-1}$]
μ_w = water liquid viscosity, [$M\,L^{-1}T^{-1}$]
ψ = soil suction, [L]
ψ_b = bubbling pressure, [L]
ρ_b = soil bulk density, [$M\,L^3$]
ρ_s = grain density, [$M\,L^3$]
ρ_{diesel} = diesel liquid density, [$M\,L^3$]
ρ_w = water liquid density, [$M\,L^3$]
σ_{diesel} = diesel surface tension, [$M\,T^{-2}$]
σ_w = water surface tension, [$M\,T^{-2}$]
θ = liquid volumetric content, [L^3L^{-3}]
θ_s = liquid volumetric content at complete saturation, [L^3L^{-3}]
θ_r = liquid volumetric content at residual saturation, [L^3L^{-3}]
Θ = effective liquid volumetric content, [–]
BTEX = benzene, toluene, ethyl-benzine and xylene
DNAPL = dense non-aqueous phase liquid
EMBASA = Empresa Baiana de Água e Saneamento
GPR = ground penetrating radar
LNAPL = light non-aqueous phase liquid
NAPL = non-aqueous phase liquid
NBR = Brazilian technical standard
SUCS = unified system of soil classification
SLRC = soil liquid retention curve
SWRC = soil water retention curve
VO = visual observations
TR = tensiometer reading
2D = two-dimensional
3D = three-dimensional

References

Abriola, L.M. (1989) Modeling multiphase migration of organic chemicals in groundwater systems: A review and assessment. Environmental Health Perspectives, v. 83, p. 117-143.

Abriola, L.M. & Pinder, G.F. (1985) A multiphase approach to the modeling of porous media contamination by organic compounds: I. Equation development. Water Resource Research, v. 21:1, p. 11-18.

Amorim Jr, C.J. (2007) Avaliação dos Critérios de Impermeabilização de Bacias de Contenção da Norma ABNT

NBR 17505-2/2006 para Terminais de Armazenamento de Petróleo e Derivados. Dissertação de Mestrado, Departamento de Engenharia Sanitária e Ambiental, Universidade Federal de Santa Catarina, Florianópolis, 114 pp.

Barreto, M.A.; Pereira, G.S.; Santos, R.E.; Machado, S.L. & Oliveira, I.B. (2007) Montagem de um canal instrumentalizado para experimentos de fluxo multifásico em solos não saturados. Proc. VI Simpósio Brasileiro de Solos Não Saturados, NSAT2007, Salvador, pp. 237-242.

Butts, M.B. & Jensen, K.H. (1996) Effective parameters for multiphase flow in layered soils. Journal of Hydrology, v. 183:1, p. 101-116.

Bond, W.J. & Collins-George, N. (1981) Ponded infiltration into simple soil systems, 1. The saturation and transition zones in the moisture content file. Soil Science, v. 131:4, p. 202-209.

Cardoso, L.P.C. (2011) Estudo do Transporte de Poluentes Orgânicos Automotivos em Solos. Tese de Doutorado, Centro Interdisciplinar de Energia e Ambiente, Universidade Federal da Bahia, Salvador, Bahia, 149 pp.

Corseuil, H.X. & Marins, M.D. (1997) Contaminação de águas Subterrâneas por derramamento de gasolina: O problema é Grave? Revista de Engenharia Sanitária e Ambiental, v. 2:2, p. 50-54.

Environmental Canada - Environmental Science and Technology Centre (1997) Diesel Fuel Oil (Southern USA, 1997). Available at http://www.etc-cte.ec.gc.ca/databases/Oilproperties/oil_D_e.html, 28/9/2010.

Host-Madsen, J. & Jensen, K.H. (1992) Laboratory and numerical investigation of immiscible multiphase flow in soil. Journal of Hydrology, v. 135, p. 13-52.

Kaipper, B.I.A. (2003) Influência do Etanol na Solubilidade de Hidrocarbonetos Aromáticos em Aquíferos Contaminados por Óleo Diesel. Tese de Doutorado, Curso de Pós-Graduação em Química, Universidade Federal de Santa Catarina, Santa Catarina, 199 pp.

Kalurachchi, K. & Parker, J. (1989) An efficient finite element method for multiphase flow. Water Resources Research, v. 25:1, p. 43-54.

Kamaruddin, S.A.; Sulaiman, W.N.A.; Rahman, N.A.; Zakaria, M.P.; Mustaffar, M. & Sa'ari, R. (2011) Journal of Environmental Science and Technology, v. 4:3, p. 191-214.

Kamon, M.; Endo, K.; Kawabata, J.; Inui, T. & Katsumi, T. (2004) Two dimensional DNAPL migration affected by groundwater flow in unconfined aquifer. Journal of Contamination Hydrology, v. 110:1-3, p. 1-12.

Kechavarzi, C.; Soga, K. & Wiart, P. (2000) Multispectral image analysis method to determine dynamic fluid saturation distribution in two dimensional three fluid phase flow laboratory experiment. Journal of Contamination Hydrology, v. 46:3-4, p. 265-293.

Kechavarzi, C.; Soga, K. & Illangasekare, T.H. (2005) Two dimensional laboratory simulation of LNAPL infiltration and redistribution in the vadose zone. Journal of Contamination Hydrology, v. 76:3-4, p. 211-233.

Kechavarzi, C.; Soga, K.; Illangasekare, T.H.; & Nicolopoulus, P. (2008) Laboratory study of immiscible contamination flow in unsaturated layered sand. Vadose Zone J., v. 7:1, p. 1-9.

Klute, A. (1986) Methods of Soil Analysis, Part 1; Physical and Mineralogical Methods. 2nd ed. Amer. Soc. Agronomy, Soil Sci. Soc. Am., Madison, 1173 pp.

Kueper, B.H.; Abbott, W. & Farquhar, G. (1989) Experimental observations of multiphase flow in heterogeneous porous media. Journal of Contamination Hydrology, v. 5, p. 83-95.

Mcdowell, C.J. & Powers, S. (2003) Mechanisms affecting the infiltration and distribution of ethanol-blended gasoline in the vadose zone. Environmental Science & Technology, v. 37:9, p. 1803-1810.

Nutting, P.G. (1934) Physical analysis of oil sands. Am. Assoc. Petroleum Geologists Bull., v. 14:10, p. 1337-1349.

Oliveira, I.B. (1995) Infiltration of Organic Liquids in Unsaturated Sands: Comparison of Experimental Measurements with Saled and Unscaled Analytical Solutions. PhD Thesis, Environmental Engineering Department, University of Michigan, Ann Arbor, Michigan, 335 pp.

Oliveira, I.B.; Demond, A.H. & Salehzadeh, A. (1996) Packing of sands for the production of homogeneous porous media. Soil Science Society of America Journal, v. 60:1, p. 49-53.

Oostrom, M.; Dane, J.H.; & Wietsma, T.W. (2007) A review multidimensional multifluid intermediate scaling experiment: Flow behavior, saturation imaging and trace detection and quantification. Vadose Zone J., v. 6:3, p. 610-637.

Philip, J.R. (1969) Theory of Infiltration. Advances in Hydroscience, v. 5, p. 215-1296.

Plagge, R.; Renger, M. & Roch, C.H. (1989) A new laboratory method to quickly determine the unsaturated hydraulic of conductivity of undisturbed soil cores within a wide range of textures. Z. Pflanzenernahr, Bodenkd, v. 153, p. 39-45.

Schiegg, H.O. (1990) Laboratory setup and results of experiments on two-dimensional multiphase flow in porous media. English translation by J.F. McBride & D.N. Graham (eds) Pacific Northwest Laboratory, October, 1990, Springfield, VA, prepared for U.S. Dep. of Energy, Washington, D.C., DE-AC06-76RLO1830, 423 pp.

Schneider, M.R. (2005) Intemperismo de Fontes de Contaminação em Aquíferos Impactados por Derramamentos de Gasolina e Álcool e a Influência sobre o Risco à Saúde Humana. Tese Doutorado, Departamento de En-

genharia Sanitária e Ambiental, Universidade Federal de Santa Catarina, Santa Catarina, 192 pp.

Schroth, M.R.; Istok, J.D.; Selker, J.S.; Oostrom, M. & White, M.D. (1998) Multifluid flow in bedded porous media: laboratory experiments and numerical simulations. Advances in Water Resources, v. 22:2, p. 169-183.

Silliman, S.E.; Berkowitz, B.; Simunek, J. & van Genuchten, M.T. (2002) Fluid flow and solute migration within the capillary fringe. Ground Water, v. 40:1, p. 76-84.

Silveira, C.S. (2004) Infiltração e Transporte de Solutos na Zona Não Saturada de um Solo Florestal - Parque Nacional da Tijuca RJ. Tese de Doutorado, COOPE, Universidade Federal do Rio de Janeiro, Rio de Janeiro, 217 pp.

Sousa, R.P.; Oliveira, I.B. & Machado, S.L. (2011) The use of hydrophobic and hydrophilic tensiometers in the measurement of water and NAPL suctions and determination of SLRC. Soils & Rocks, v. 34:3, p. 251-259.

Tamari, S.; Bruckler, L.; Halbertsma, J. & Chadoeuf, J. (1993) A simple method for determining soil hydraulic properties in the laboratory. Soil Sci. Soc. Am J., v. 57:3, p. 642-651.

van Genuchten, M.T. (1980) A closed form equations for predicting the hydraulic conductivity of unsaturated soils. Soil Science Society of America Journal, v. 44:5, p. 892-898.

Wendroth, O.; Ethlers, J.; Hopmans, J.W.; Kage, H.; Halbertsma, J.; & Wosten, J.H.M. (1993) Reevaluation of the evaporation method for determining hydraulic functions in unsaturated soils. Soil Science Society of America Journal, v. 57:6, p. 1436-1443.